Numerical investigation of a looped-tube travelling-wave thermoacoustic engine with a bypass pipe

Ali Al-Kayiem and Zhibin Yu*

School of Engineering, University of Glasgow, Glasgow, United Kingdom

*Corresponding Author, Email: Zhibin.Yu@glasgow.ac.uk

Abstract

A new configuration ("a looped-tube with a bypass pipe") was recently proposed for low temperature travelling wave thermoacoustic engines and a prototype using atmospheric air as the working gas achieved an onset temperature difference as low as 65 °C. However, no further research has been reported about this new configuration to reveal its advantages and disadvantages. This paper aims to analyse this type of engine through a comprehensive numerical research. An engine of this type having dimensions similar to the reported prototype was firstly modelled. The calculated results were then qualitatively compared with the reported experimental data, showing a good agreement. The working principle of the engine was demonstrated and analysed. The research results show that an engine with such a bypass configuration essentially operates on the same thermodynamic principle as other travelling wave thermoacoustic engines, differing only in the design of the acoustic resonator. Both extremely short regenerators and a near-travelling wave resonator minimise the engine's acoustic losses, and thus significantly reduce its onset temperature difference. However, such short regenerators likely cause severe heat conduction losses, especially if the engine is applied to heat sources with higher temperatures. Furthermore, the acoustic power flowing back to the engine core is relatively low, while a large stream of acoustic power has to propagate within its resonator to maintain an acoustic resonance, potentially leading to low power density. The model was then applied to design an engine with a much longer regenerator and higher mean pressure to increase its power density. A thermoacoustic cooler was also added to the engine to utilise its acoustic power, allowing the evaluation of thermal efficiency. The pros and cons of the engine configuration are then discussed.

Keywords: **Thermoacoustic engine, Travelling wave, bypass configuration, Thermoacoustic cooler**

1. Introduction

Thermoacoustic systems can either generate acoustic work (i.e., p-v work) from thermal energy, or consume acoustic work to transfer heat from low to high temperature. They are the so-called thermoacoustic prime movers or heat pumps, respectively. Essentially, they are acoustical equivalents of Stirling engines or coolers. In 1979, Ceperley [2, 3] revealed that, when a travelling sound wave propagates through a regenerator with a positive temperature gradient along the direction of sound wave propagation, the gas parcel experiences a Stirling-like thermodynamic cycle. As such, thermal energy can be converted to acoustic power. Based on this concept, Yazaki et al. [4] demonstrated the first travelling wave thermoacoustic engine which has a thermoacoustic engine core (i.e., a regenerator sandwiched by a pair of cold and hot heat exchangers) in a one-wavelength looped-tube resonator. Backhaus and Swift [5] later developed a travelling wave thermoacoustic Stirling engine which placed the engine core within a torus with a length much shorter than one acoustic wavelength at the operating frequency. A quarter-wavelength standing wave resonator was connected to the torus to provide acoustic resonance. This engine achieved a thermal efficiency of 30%, equivalent to 41% of the theoretical Carnot efficiency. Tijani and Spoelstra [6] later built and tested an engine of this type, and reported that 49% of the Carnot efficiency was achieved.

De Blok made a series of efforts to develop various travelling wave thermoacoustic engines [1, 7-9]. He proposed a traveling-wave thermoacoustic engine with coaxial configuration in 1998 [7]. In 2008, he proposed a new configuration (i.e., a looped-tube with a bypass pipe) for a travelling wave thermoacoustic engine, which achieved an onset temperature difference as low as 65 °C [1]. It is denoted as “bypass configuration” hereafter in this paper. Later, he also developed multistage looped-tube travelling wave thermoacoustic engines, and applied them to drive a cooler or linear alternator for different applications [8, 9].

Similar to Stirling engines [10] and thermo-fluidic oscillators [11], thermoacoustic engines can be externally heated with various heat sources and are capable of utilising low grade thermal energy such as industrial waste heat and solar thermal energy. Owing to their simplicity and absence of moving parts, travelling wave thermoacoustic engines have the potential for developing low-cost power generators and thus have attracted much research effort for developing coolers [12-17] or electric generators [18-34].

In the past decades, great efforts have been made to develop thermoacoustic generators with different configurations and transducers [18-34]. In 2004, Backhaus et al. developed the first

traveling wave thermoacoustic electric generator based on a flexure-bearing linear alternator for deep space application. At its most efficient operating point, the system generated 39W electric power at a thermal-to-electric efficiency of 18% [18, 19]. In 2008, Sunpower Inc. developed a coaxial traveling wave thermoacoustic electric generator, which achieved an electric power output of 50W [20]. Wu et al. constructed a traveling-wave thermoacoustic electric generator that produced 481W electric power with an efficiency of 15% [21]. Later on, this group developed a solar powered thermoacoustic electric generator which delivered about 200W electricity [22]. In 2013, based on a flexure-bearing linear alternator, Sun et al. developed a traveling-wave thermoacoustic electric generator using helium at 3.0 MPa as the working gas, which achieved a maximum electric power of 345.3W with a thermal-to-electric efficiency of 9.3% [23]. In 2014, Wu et al. developed a double-acting thermoacoustic Stirling electric generator which had three thermoacoustic Stirling engine stages and three linear alternators. Using 5 MPa pressurised helium as working gas, the prototype achieved a maximum electric power of about 1.57 kW and a maximum thermal-to-electric conversion efficiency of 16.8% [25]. In 2016, this group increased the power generation of their three-stage travelling wave thermoacoustic electric generator to 4.69 kW [26]. Wang et al. [27, 28] also developed and tested two prototypes of thermoacoustic electric generators that were driven by Backhaus and Swift type travelling wave thermoacoustic engines, and achieved promising results.

Along with the development of thermoacoustic generators based on flexure-bearing linear alternators, efforts have also been made to develop inexpensive systems using ultra-compliant linear alternators (e.g., audio loudspeakers) as transducers [29-34]. Yu et al. developed a small-scale inexpensive prototype generator using atmospheric air as the working gas and a six-inch B&C subwoofer as an alternator, and it produced 11.6W of electrical power [30]. Kang et al. reported a two-stage travelling wave thermoacoustic electric generator using two audio loudspeakers as transducers which generated 204 W electricity. This demonstrated the feasibility of developing inexpensive thermoacoustic electric generators [31].

Despite the different engine configurations for developing these engines, they all work on the same thermodynamic principle, i.e., the Stirling cycle. The difference mainly lies in the different design of the resonator which can be an acoustic resonator, mechanical resonator, or a combination of both. Similar to the flywheel of a Stirling engine, the resonator provides acoustic resonance to enable the gas parcel to complete the thermodynamic cycle within the regenerator. Depending on the characteristics of the acoustic field within the resonator, it can

be a standing wave or travelling wave resonator. Backhaus' thermoacoustic Stirling engine used a quarter-wavelength standing wave resonator [5]. Yazaki's engine [4] used a one-wavelength travelling wave resonator. De Blok's' bypass type engine used a travelling wave feedback pipe with a bypass pipe [1]. In his multistage engine, several engine stages share a one-wavelength resonator, leading to better performance [9]. The thermoacoustic generator developed by Backhaus et al. had a mechanical resonator [18, 19]. All the other electric generators [21-34] have a combined resonator system.

In general, the design principle of a thermoacoustic engine is to maximise the acoustic power production within the thermoacoustic core, while minimising the loss associated with the acoustic power transmission. A travelling wave resonator is superior to a standing wave one because its acoustic loss is much lower [8, 9]. Hence, the development of suitable travelling wave resonators remains a hot research topic. As schematically shown in Figure 1, the thermoacoustic engine with a bypass configuration developed by de Blok achieved a very low onset temperature difference, which was attributed to the novel design of the resonator. [1] However, the heat power input to the prototype, its net acoustic power production, and its thermal efficiency were not reported in the reference [1]. It is therefore unknown how efficient the prototype was. This is indeed a very interesting and important question. Moreover, there is no further research on this type of engine to analyse its advantages and disadvantages. It also remains unknown if the regenerator length can be increased, without violating the working principle, to utilise heat sources with higher temperatures.

This paper aims to answer these questions through comprehensive numerical research. Firstly, using the DeltaEC programme [35], an engine with this bypass configuration is modelled based on the information of the prototype reported in the reference [1], and the simulations are then qualitatively compared with reported experimental data. The working principle is demonstrated and analysed. The model is then used to design an engine with a much longer regenerator and higher mean pressure to increase its power density. A thermoacoustic cooler is also added to the engine as an acoustic load so that the thermal efficiency can be evaluated numerically. Finally, the pros and cons of this bypass configuration are analysed and discussed.

2. Modelling and simulations of a bypass engine

A travelling wave thermoacoustic engine with the bypass configuration (see Figure 1) is modelled using DeltaEC software (Design Environment for Low-amplitude ThermoAcoustic Energy Conversion) [35, 36]. It is denoted as a bypass engine hereafter. The purpose of this modelling is to qualitatively capture and demonstrate the working principle of this type of engine [1] rather than to reproduce the prototype accurately.

As shown in Figure 1, this engine has two stages, and each stage has a hot heat exchange (HHX), a regenerator (REG), and an ambient heat exchanger (AHX). The system also has a feedback pipe, a bypass pipe, a compliance volume, and a “phase shifting pipe”. It should be noted that the “phase shifting pipe” was denoted as an “inertance tube” in the reference [1]. As explained later on in this paper, the inertance tube, widely used in pulse-tube coolers, usually has a very small cross-sectional area and long length to provide a significant phase shifting effect [37]. Strictly speaking, the pipe that connects the compliance volume and the engine core in the reference [1] does not have the characteristics of an “inertance pipe”, and therefore is denoted as a “phase shifting pipe” instead in this paper.

It should be noted that, like other travelling wave thermoacoustic engines, there are torus paths within this bypass configuration. As a result, Gedeon streaming, a second-order time-averaged mass flow, will be induced along the loop. In such a system, such a mass flow can take heat from the hot heat exchanger of the engine and dump it at the ambient heat exchanger, causing heat loss and reducing the thermal efficiency [5]. It is a well understood effect, can be supressed using a jet-pump [5] or elastic membrane [36]. In this paper, it is assumed that the Gedeon streaming has been supressed in order to simplify the analysis.

Some dimensions and operating parameters of the prototype were reported in the paper and the associated conference presentation. [1] The working gas was air at atmospheric pressure. The operating frequency was 119 Hz. The heat source temperature was 148 ℃, and the heat sink temperature was 28 ℃. The heat exchangers of the prototype were made by soldering several lays of copper mesh screen to copper water tubes. The regenerators were made of stainless steel mesh discs. [1]

These reported dimensions and operating parameters are used as a basic framework to establish the present DeltaEC model. Screen-type heat exchangers (i.e., SX) and regenerators (i.e., STKSCREEN) have been used in the model. Some unreported parameters are then carefully tuned to force the model to closely approach the reported experimental data including the pressure amplitude at location P2, and the acoustic power measured at locations P1 and P2 (see Figure 1). The final dimensions used in this model are summarised in Table 1. It should be noted that these dimensions might be different from those of the actual prototype reported in the reference because the DeltaEC model could possibly converge to the same boundary conditions using different combinations of the unknown parameters. Nevertheless, such an approximation is acceptable and enough for us to qualitatively demonstrate the working principle of this bypass type of engine.

Based on the obtained model, the distribution of pressure amplitude, volumetric velocity, normalised specific acoustic impedance, and phase angle between the pressure and velocity oscillations are then calculated and presented in Figures 2-5. The coordinate x starts from (and also ends at) Junction 1 as shown in Figure 1. For the convenience of presentation, the feedback pipe and engine branch form the main loop for plotting the experimental data.

As reported in the reference [1], the pressure amplitude at location P2 in the resonator (see Figure 1) was measured as 3430 Pa. According to our estimation, the location P2 is about 15-25 cm away from Junction 2. For the convenience of comparison, the pressure amplitude is set to 3430 Pa at the location P2 in the present model. Figure 2 shows the calculated pressure amplitude along the main loop (solid line) and bypass pipe (dashed line with symbols). The measured pressure amplitude at location P2 (see Figure 1) in the reference [1] is also represented by a solid square in Figure 2. The horizontal error bar shows the uncertainty of the location of P2 due to our estimation.

Figure 3 shows the acoustic power flow along the system according to the present model. The simulation starts from the Junction 1 where x=0. The total acoustic power is around 80 W, and it splits into two parts. One part (about 47 W) flows into the bypass pipe, and the other part (about 33 W) flows into the compliance volume. The compliance volume and phase shifting pipe dissipate about 2 W, and the remaining 31 W power flows into the first engine stage. The two engine stages slightly amplify the acoustic power to 37 W, which then joins with the acoustic power (45 W) exiting from the bypass pipe. The total power of about 82 W

flows into the feedback pipe. About 2 W of acoustic power has been dissipated in the feedback pipe and the remaining 80 W flows back to starting point (x=0).

In the reference [1], acoustic power was measured at two locations, P1 and P2, as schematically shown in Figure 1. Location P1 lies in the centre of the phase shifting pipe and location P2 is located about 15-25 cm away from the Junction 2. The measured acoustic power was about 35 W at location P1 and about 78 W at location P2. As shown in Figure 3, in the present model, the calculated acoustic power is 32 W and 79 W at location P1 and P2, respectively, showing a reasonably good agreement.

As described above, the present model is based on a large number of parameters and dimensions of the actual prototype. In addition, the calculated pressure at P2 and acoustic power at P1 and P2 are forced to approach the measured data by tuning other unknown dimensions. It could therefore be inferred that this model approximately represents the actual prototype. Based on this model, we can then check if it demonstrates the working principle as described in the reference [1].

As reported in the reference [1], the design principle of the prototype was that, the specific acoustic impedance at the end of the feedback pipe (x=0 or 3.1 m) should be tuned to the characteristic impedance $\rho_m a$ for air at atmospheric pressure, so that the acoustic reflection within the feedback pipe can be minimised. As such, the acoustic power can be transmitted through the feedback pipe with the least losses [1]. Here, the specific acoustic impedance is defined as ratio of acoustic pressure $p_1$over acoustic velocity u_1, z=p_1/u_1 [36].

To check this principle in the present model, the normalised specific acoustic impedance $|z|/\rho_m a$ has been calculated and presented in Figure 4. It can be found that $|z|/\rho_m a$ at the end of the feedback pipe (x=3.1 m) is about 0.7, which is close to the target value of 1 proposed in reference [1]. The value of $|z|/\rho_m a$ increases along the compliance volume from 2.45 to 4, and then sharply drops to 0.7 at the start of the phase shifting pipe due to a sudden change of cross sectional area. It is in the range 4.6-5.4 around the two regenerators of the prototype (see Fig. 4). According to reference [1], it was estimated to be in the range 4.1-6.1 around the two regenerators but no measurement was reported. This again shows a good agreement between the two studies, indicating that the present model has captured the essence of the prototype. Furthermore, $|z|/\rho_m a$ is in the range 0.6-1.4 within the feedback pipe, which is very

close to the ideal value of 1 as proposed in the reference [1]. As expected, $|z|/\rho_m a$ is close to 1 throughout the bypass pipe.

To further check the working principle of this bypass engine, the phase difference between the pressure and velocity oscillations has been calculated and shown in Figure 5. The compliance volume section shifts the phase significantly from -56° to about -8°. However, the phase shifting pipe (the so-called "inertance tube" in the reference [1]) works like a section of feedback pipe. The phase shifting effect is insignificant. This is not a surprise because its diameter is 50 mm, which is comparable to the diameter of the feedback pipe (i.e., 75 mm). For this reason, it does not have the characteristics of a typical inertance tube, and therefore it is denoted as phase shifting pipe in this paper.

Since the regenerator and the heat exchangers have a high porosity and a much larger cross-sectional area than the phase shifting pipe, their large volumes introduce a strong compliance effect. As a result, the phase angle has been sharply shifted from 18° to 39° within the engine core section as shown in Figure 5. This is similar to a typical looped-tube travelling wave thermoacoustic engine [16]. The phase angle is then shifted back to around 12° where the bypass pipe re-joins with the engine branch at Junction 2. Thereafter, the phase angle changes gradually along the feedback pipe as expected.

3. Discussion on the bypass configuration

According to Figure 3, the directions of the acoustic power flow are then schematically shown in Figure 1. Air is the working gas and the speed of sound is around 343 m/s at room temperature. As the operating frequency is 119 Hz, the wavelength is estimated as 288 cm. According to Table 1, the lengths of bypass pipe and feedback pipe are 100 and 175 cm, respectively. Hence the total length of the loop formed by these two components is about 275 cm which is very close to the sound wavelength under these conditions. Furthermore, according to Figure 5, both the by-pass (dashed line with symbols) and the feedback pipe have a phase angle in the range $-22° < \Theta < 22°$, and thus a near travelling wave field has been achieved in these two components. From the acoustic viewpoint, these two components seem to form a near-travelling wave acoustic resonator for the engine.

Following the analysis above, the engine branch (including the compliance, the phase shifting pipe, and the engine core) extracts a part (i.e., <50%) of the acoustic work from the resonator, slightly amplifies it within the engine core, and then injects it back to the resonator. The compliance volume and the phase shifting pipe both provide the required phase shifting for the engine core to operate in a right phase condition. As the travelling wave resonator has low losses, it requires little acoustic power to sustain an acoustic resonance, leading to low onset temperature difference.

The short regenerator length (<2 mm) is another special design of the prototype. According to the linear thermoacoustic theory [35-36, 38], the time-averaged acoustic power $d\dot{E}_2$ produced in length dx of a stack-screen regenerator can be approximately written as [38, 39]

$$\begin{aligned}\frac{d\dot{E}_2}{dx} = \frac{1}{2}A_g\,\mathrm{Re}\Bigg\{ & i\omega\left[\beta_m\frac{T_m\beta_m}{\rho_m c_{p,m}}\frac{\varepsilon_s+\left(g_c+e^{2i\theta_p}g_v\right)\varepsilon_h}{1+\varepsilon_s+\left(g_c+e^{2i\theta_T}g_v\right)\varepsilon_h}-\frac{\gamma_m}{\rho_m a_m^2}\right]\left|p_1\right|^2 \\ & -i\omega\rho_m\left|\langle u_1\rangle\right|^2-\frac{\mu_m}{r_h^2}\left[\frac{c_1(\phi)}{8}+\frac{c_2(\phi)Re_1}{3\pi}\right]\left|\langle u_1\rangle\right|^2+\beta_m\frac{dT_m}{dx}\left[1-\frac{\varepsilon_s+\left(g_c-g_v\right)\varepsilon_h}{1+\varepsilon_s+\left(g_c+e^{2i\theta_T}g_v\right)\varepsilon_h}\right]\tilde{p}_1\langle u_1\rangle\Bigg\}\end{aligned} \tag{1}$$

In equation (1), A_g is the cross-sectional occupied by working gas, Re{ } denotes the real part of a complex variable, and ⟨ ⟩denotes a local spatial average. β_m, γ_m and μ_m are mean thermal expansion coefficient, mean ratio of specific heats, and mean dynamic viscosity of the gas, respectively. $b(\emptyset)$ $c_1(\emptyset)$, $c_2(\emptyset)$, $g_c\left(R_{e_1}\right)$ and $g_v\left(R_{e_1}\right)$ are factors resulting from the fitting of data of Kays and London [40]. θ_p and θ_T are defined as $\theta_p=\theta\left(p_1,\langle u_1\rangle\right)$ and $\theta_T=\theta\left(\langle u_1\rangle,\langle T\rangle_{u,1}\right)$, respectively. $\varepsilon_s=\phi\rho_m c_{p,m}/\left(1-\phi\right)\rho_{s,m}c_{s,m}$ (subscript s means solid) gives the ratio of gas heat capacity to solid heat capacity in the stacked screen regenerator. ε_h is defined as $\varepsilon_h=8ir_h^2/b(\phi)\sigma^{1/3}\delta_k^2$. Reynolds number $Re_1=4\left|\langle u_1\rangle\right|r_h\rho_m/\mu_m$ is a positive real number [38].

In the curly brackets at right hand side of equation (1), the first term represents the acoustic power dissipation due to thermal relaxation effects, the second and third terms together represent the acoustic power dissipation due to the flow resistance in the regenerator, and the fourth term is the acoustic power generation from thermal energy through thermoacoustic effect. Integrating the right hand side of equation (1) over the length of the regenerator L leads to the total net acoustic power generation by the regenerator as

$$\Delta\dot{E} = \frac{1}{2}\int_0^L A_g \mathrm{R_e}\left\{i\omega\left[\beta_m \frac{T_m\beta_m}{\rho_m C_{p,m}} \frac{\varepsilon_s+(g_c+e^{2i\theta_p}g_v)\varepsilon_h}{1+\varepsilon_s+(g_c+e^{2i\theta_p}g_v)\varepsilon_h} - \frac{\gamma_m}{\rho_m a_m^2}\right]|p_1|^2 - i\omega\rho_m|\langle u_1\rangle|^2 - \right.$$

$$\left.\frac{\mu_m}{r_h^2}\left[\frac{c_1(\emptyset)}{8}+\frac{c_2(\emptyset)R_{e_1}}{3\pi}\right]|\langle u_1\rangle|^2 + \beta_m\frac{dT_m}{dx}\left[1-\frac{\varepsilon_s+(g_c-g_v)\varepsilon_h}{1+\varepsilon_s+(g_c+e^{2i\theta_T}g_v)\varepsilon_h}\right]\tilde{p}_1\langle u_1\rangle\right\}dx \quad . \tag{2}$$

In order to further demonstrate the effect of the length of a regenerator on the power production within it, neglecting the dissipations due to thermal relaxation and viscosity in Equation (2) leads to

$$\Delta\dot{E} \cong \frac{1}{2}A_g\beta_m\int_0^L \mathrm{R_e}\left\{\left[1-\frac{\varepsilon_s+(g_c-g_v)\varepsilon_h}{1+\varepsilon_s+(g_c+e^{2i\theta_T}g_v)\varepsilon_h}\right]\tilde{p}_1\langle u_1\rangle\frac{dT_m}{dx}\right\}dx \quad . \tag{3}$$

According to equation (3), we can see that the acoustic power production from the regenerator strongly depends on the length of the regenerator L, the temperature gradient $\frac{dT_m}{dx}$, and the term $\tilde{p}_1\langle u_1\rangle$ that is related to the acoustic power flowing into the regenerator. Qualitatively speaking, in order to increase the acoustic power production from a regenerator, we should increase the regenerator length, the temperature gradient, or the acoustic power flowing into the cold end of the regenerator. However, these parameters are strongly dependent on one another. For instance, the average temperature gradient along the regenerator depends on the length of the regenerator and can be defined as

$$\frac{dT_m}{dx} = \frac{T_H - T_L}{L}, \tag{4}$$

where T_H and T_L are the temperatures at the hot and cold end of the regenerator, respectively. According to equation (4), for a given temperature difference, the temperature gradient decreases as the regenerator length increases. Therefore, in a practical design, a trade-off is needed to obtain an optimal regenerator length when the temperature difference is given.

Looking back to the prototype [1], for the very low temperature heat sources, the temperature differential between the two ends of the regenerator is very small. Therefore, the regenerator length has to be very short to achieve a sufficient temperature gradient for a positive net power production according to equation (2). The net power generation of one engine stage may be still too low since the regenerator length is so short. In order to generate enough acoustic power to maintain the acoustic oscillation, the prototype was designed with two engine stages [1].

As analysed above, both the travelling wave resonator and short regenerators are likely the reasons behind the extremely low onset temperature difference achieved by the bypass engine prototype. Overall, it is a very successful design strategy to reduce the engine's onset temperature difference. However, as a power generator, two important performance parameters are power density and thermal efficiency. We will continue to analyse if there are any drawbacks due to this bypass engine configuration.

Firstly, as shown in Figure 3, the net power production by the two engine stages is only 6 Watts, while the acoustic power flow within the resonator is about 80 Watts, leading to a low power density. This problem will get even worse if gas with high speed of sound (e.g., helium) is used as working fluid because the total length of the loop is around one wave-length.

Secondly, in the prototype [1], the regenerator is around 1.58 mm in length, while the calculated temperature difference between the two ends of the regenerators is over 100 °C. As a result, the axial temperature gradient along the regenerator is over 60,000 °C/m. This is extremely high. For reference, in Backhaus and Swift's travelling wave Stirling engine, the temperature difference is about 600-700 °C and the regenerator length is 8.89 cm [5], so the temperature gradient along the regenerator is in the range 6750-7874 °C/m. The temperature gradient along the regenerators of the prototype is 10 time higher than that in Backhaus and

Swift's engine. Apparently, such an extremely short regenerator will potentially cause severe heat conduction losses from the hot heat exchanger to the ambient heat exchanger through the regenerator. Such heat loss will increase dramatically if we increase the temperature difference to increase power production. To reduce such heat conduction loss, the regenerator length has to be increased to ensure the temperature gradient is in a reasonable range.

The heat power input to the prototype, its net acoustic power production, and its thermal efficiency were not reported in the reference [1]. It is therefore unknown how efficient the prototype was. This however is a very interesting and important question. In the present model, the temperatures of the hot heat and cold heat exchanger are kept the same as those in the experiments. Under these conditions, the calculated heat input to each hot heat exchanger is around 600 W, and thus the total heat energy input is 1200 W. As shown in Figure 3, the total net acoustic power generation is about 6 W. If we roughly assume this net power production as the engine's power output, the thermal efficiency of the modelled engine is estimated around 0.5%.

It should be noted that we have used idealised Screen-type heat exchangers in our model, which are assumed to have perfect heat transfer between the working gas and the metal surface of the heat exchanger. The actual heat exchangers in the prototype were made by soldering a few lays of copper mesh to copper tubes [1]. They heat transfer to the working gas would be much lower than the prediction based on the idealised Screen-type heat exchangers in our simulation. Therefore, the actual efficiency of the prototype, which was not reported, should be a higher than our predictions here.

Nevertheless, in order to make this type of engine technically attractive, both its power density and thermal efficiency need to be better than, or at least as good as other travelling wave thermoacoustic engines. A few things can be done. Firstly, the charging pressure can be increased. For instance, Backhaus and Swift's thermoacoustic Stirling engine used helium at 30 bar as working fluid [5]. Luo's thermoacoustic generators used helium at 50 or 60 bar as working gas [25, 26]. Secondly, the temperature of the heat source can be increased and the regenerator length needs to be increased accordingly. Alternatively, if the heat source temperature is low, the number of engine stages can be increased. This however will increase the number of heat exchangers which are expensive and bulky. Hence, increasing the regenerator length and mean pressure seem to be more feasible. It is however unclear if such

modifications would violate the working principle as discussed above. In the next section, we will investigate these problems.

4. Application to a thermoacoustic engine driven cooler

In this section, we will investigate how to improve the power density and thermal efficiency of this bypass type engine without violating its working principle. We apply this bypass configuration to design a thermally driven thermoacoustic refrigerator with a cooling temperature at about -20 ℃. The targeted waste heat source is the exhaust gas of vehicle engines, which has a temperature in the range of 200-300 ℃. The ambient temperature is set to 28 ℃. The whole system has the same configuration as that shown in Figure 1. However, the second engine unit is replaced by a cooler stage, and the regenerator of the engine stage has been increased from 1.58 to 10 mm to utilise such heat source. The working gas is nitrogen at 10 bar. The operating frequency is reduced to about 76.5 Hz according to the availability of stainless steel mesh screen.

The dimensions of the main components are summarised in Table 2. The regenerators are made of stainless steel mesh screen. All of the heat exchangers have a tube-and-shell configuration which is simpler for manufacturing than the idealised Screen-type heat exchanger. In Table 2, AHX1, REG1 and HHX1 form the engine unit, while AHX2, REG2 and CHX2 form the cooler unit. In de Blok's prototype, the gap between the two engine stages is only about 3 cm to act as a thermal buffer tube due to the low temperature of the heat source. In this system, the temperature difference between HHX1 and AHX2 is about 230 ℃, and therefore, its length is increased to 19 cm to reduce the heat losses from the hot heat exchanger of the engine stage to the ambient heat exchanger of the cooler stage.

4.1 Optimisation results

The optimisation of this thermoacoustic engine driven cooler involved a large number of parameters. A few typical steps are presented here to demonstrate the optimisation process of this complicated system. For each round of optimisation, one parameter is swept in a range when the rest of the parameters are kept constant. The lengths of the regenerator, bypass pipe, phase shifting pipe, compliance volume and thermal buffer tube are important design parameters, and therefore are selected to demonstrate the optimisation processes.

Figure 7 shows the effect of the regenerator length of the engine stage on the efficiency. Here, the engine efficiency is defined as the ratio of the acoustic power consumption of the cooler over the heat input to the engine. It can be found that there is an optimal regenerator length about 10 mm, and it is selected for the fianl design as sumarrised in Table 2. The regenerator length is crucial. On one hand, its flow reistance increases when the length increases, leading to high acoustic losses. On the other hand, according to equation (2), the acoustic power production is approximatly propotional to the temperature gradient. For a given temperature difference, the longer the length, the smaller the temprature gradient. Fruthermore, the shorter the length, the higher the conductive heat loss through the regenerator. Therefore, a very careful trade-off is required.

Figure 8 shows the relationship between the engine efficiency and length of the bypass pipe length. The optimal length is about 100 cm and it is selected for the final design. Similarly, Figure 9 shows the relationship between the length of the phase shifting pipe and engine efficiency. The optimal length is about 120 cm, and it is selected for the final design. Figure 10 shows the effect of the length of the compliance volume on the engine efficiency. Compared with other parameters, it has a relatively weak effect on the engine efficiency. In the final optimised model, the length of the compliance volume is selected as 12.7 cm. The bypass pipe, compliance volume and phase shifting pipe are all the phase control components. Their dimensions are important for achieving the right phase and impedance within the engine and cooler units, as well as in the feedback pipe.

Figure 11 shows the engine efficiency as a function of the length of the thermal buffer tube when the other parameters are kept unchanged. It can be found from this figure, its length affects the engine efficiency slightly. It is selected as 19 cm in the final model. In practice, it

provides a thermal buffer between the hot heat exchanger and room temperature. Its length should be much greater than the local gas displacement. In the present model, the local gas displacement amplitude is around 3 cm in this system. The length of the TBT is about 6 times as this displacement, which is in line with the arrangement of Backhaus and Swift's thermoacoustic Stirling engine [5].

4.2 The optimised model

In the optimised model, the maximum pressure amplitude is about 54 kPa, and therefore the relative pressure amplitude to the mean pressure is about 5.4% which meets the low amplitude criteria to use the DeltaEC software. The whole system is schematically shown in Figure 6. The simulation results of the optimised model are summarised in Table 3. The heat source temperature (i.e. the solid temperature at HHX1) is set as 260 °C, and the heat sink temperature (i.e., the solid temperature of AHX1 and AHX2) is 28 °C. The net acoustic power production from the engine unit (i.e., the difference between its inlet and outlet acoustic power) is about 195.8 W. The acoustic power consumed by the cooler is 159.5 W. The heat input to the engine's hot heat exchanger is 1100.7 W. The thermal efficiency η_e, defined as the ratio of the acoustic power consumed by the cooler over the heat input to the engine, is 14.5%. It is equivalent to 33.3% of the Carnot efficiency for the same heat source and sink temperatures. The cooler removes 232.4 W heat at -19.1 °C, and rejects it at 28 °C. The cooler's coefficient of performance (COP) is defined as the ratio of the heat absorbed at CHX2 over the acoustic power it consumes. The calculated COP is about 1.46, equivalent to 27% of the Carnot COP at this temperature range. The performances predicted by this model are comparable to multi-stage travelling wave thermoacoustic systems under similar conditions. [16, 41]

The details of the acoustic field within the system have been calculated and shown in Figures 12-16 to further investigate the final design. In the figures, the solid line represents the results for the engine loop (i.e., engine branch and feedback pipe), and the dashed line with symbols represents the results of the bypass pipe.

Figure 12 shows the distribution of the acoustic pressure amplitude along the system. The maximum pressure amplitude is 54 kPa at the engine core and the minimum pressure amplitude is 27 kPa at the middle of the bypass pipe, so the maximum-to-minimum ratio [1] is about 2 in the whole system, which is slightly higher than 1.2 in de Blok's prototype. This is mainly due to the regenerator length having been increased to 10 mm, and therefore the flow resistance at the engine core is higher and thus the acoustic reflection is higher. In the feedback pipe, the maximum pressure amplitude is about 52 kPa, and the minimum amplitude is about 36 kPa, so the maximum-to-minimum ratio is about 1.4 which is very close to 1 in the ideal travelling wave condition.

Figure 13 shows the distribution of the amplitude of volumetric velocity along the system. It can be seen that the bypass pipe shunts away more than half of the volumetric velocity at the location x=0. As a result, more than half of the acoustic power (i.e., 512 W) flows to the bypass and only 428 W acoustic flows into the engine branch. There is a sharp increase of volumetric velocity at the regenerator of engine stage due to the steep temperature gradient along the regenerator. The other sharp increase is due to the bypass pipe joining after the end of the cooler.

Figure 14 shows the normalised specific acoustic impedance along the system. To reduce the acoustic losses with in the regenerator, the specific acoustic impedance $|z|$ should be designed

in the range of 15-30 times of $\rho_m a$ [5]. In the present model, it can be seen that the value of $|z|/\rho_m a$ in most parts of the system is around 1 except the engine and cooler sections where it is 9.6 and 8.4, respectively. It should be noted that, in order to achieve a very low onset temperature difference, de Blok's prototype has low impedance within the regenerators due to the short regenerators. In our design, we substantially increased the regenerator length to use a heat source with a higher temperature. Therefore, the resultant system has relatively higher impedance in the regenerator.

Figure 15 shows the phase difference between pressure and velocity oscillations along the loop. It can be found that phase angle is in the range $-20° < \Theta < 20°$ in the feedback pipe, engine unit, and cooler, as expected. The rest of the system also has a phase angle in the range $-40° < \Theta < 40°$. Therefore, the whole system works in near travelling wave conditions as expected.

Figure 16 shows the acoustic power flow along the system. The simulation starts from the Junction 1 (x=0). At this point, the 940 W of acoustic power is divided into two parts, one part (~512 W) flows into the bypass and the other part (~428 W) flows into the compliance volume section. About 420 W of acoustic power is fed into the engine core which is then amplified to around 613 W. There is a small amount of acoustic loss (around 1.35 W) along the thermal buffer tube. The cooler unit consumes around 159.5 W. Around 452 W of acoustic power exits the cooler and joins with the acoustic power flow from the bypass pipe (~504 W) at the Junction 2. In total, about 956 W of acoustic power then flows into the feedback pipe. The feedback pipe transmits the acoustic power back to the starting point (x=0) after about 10 W of acoustic power is dissipated. The ratio of the power flows to the bypass and engine branch is quite similar to that in de Blok's prototype.

The results presented in this section suggest that the working principle of de Blok's bypass engine can be achieved after the regenerator length and mean pressure are substantially increased. As such, the system's power density and thermal efficiency can be improved. The modelled thermoacoustic engine driven cooler predicted a performance similar to systems having other configurations. The future work should be focused on the experimental verification.

5. Conclusions

This paper presents comprehensive numerical research of a travelling wave thermoacoustic engine with a bypass configuration and its applications to thermoacoustic engine driven coolers.

Based on the reported dimensions and operating parameters, an engine of this type was modelled to qualitatively represent this prototype. The working principle was then demonstrated and analysed. According to the results, this type of engine essentially operates on the same thermodynamic principle as other travelling wave thermoacoustic engines, differing only in the design of the acoustic resonator. Its feedback pipe and bypass pipe seem to form a travelling wave resonator. Both the travelling wave resonator and two stages of engines with very short regenerators are effective measures to significantly reduce the engine's onset temperature difference.

The acoustic power fed back to the engine branch is low because the bypass pipe shunts more than half of the power flow away. As a result, the net acoustic power production from the engine core is relatively low. The short regenerator is useful for utilising low temperature heat sources, but it also limits the power generation capacity and potentially causes severe heat conduction losses. Both of these two features could lead to a low power density and low thermal efficiency.

To improve the power density and thermal efficiency, the regenerator length and mean pressure can be increased. The model was then applied to design a thermoacoustic engine driven thermoacoustic cooler with much longer regenerator and higher mean pressure. The

design principle contained in the bypass type engine was successfully implemented in the design. It is inferred that a longer regenerator length is possible for this bypass engine configuration. The model of the thermoacoustic engine driven cooler predicts similar performance with those systems having other configurations. The future work would be focused on the experimental verification and demonstration.

ACKNOWLEDGMENT

Ali Al-Kayiem appreciates support from the Ministry of Higher of Education/ Babylon University in Iraq (No. 553, Iraqi cultural attaché).

References

[1] De Blok K. Low operating temperature integral thermo acoustic devices for solar cooling and waste heat recovery. Journal of the Acoustical Society of America 2008; 123(5): 3541-3541. And the presentation associated with this paper available on http://www.aster-thermoacoustics.com

[2] Ceperley PH. A pistonless Stirling engine-The traveling wave heat engine. The Journal of the Acoustical Society of America 1979; 66:1508.

[3] Ceperley PH. Gain and efficiency of a short traveling wave heat engine. The Journal of the Acoustical Society of America 1985; 77:1239.

[4] Yazaki T, Iwata A, Maekawa T, Tominaga A. Traveling wave thermoacoustic engine in a looped tube. Physical Review Letters 1998; 81(15):3128.

[5] Backhaus S, Swift G. W. A thermoacoustic-Stirling heat engine: Detailed study. The Journal of the Acoustical Society of America 2000; 107**,** 3148.

[6] Tijani MEH, Spoelstra S. A high performance thermoacoustic engine. J ApplPhys 2011; 110:093519.

[7] De Blok CM. Thermoacoustic system Dutch patent. International application number PCT/NL98/00515; 1998.

[8] De Blok Kees. Multi-stage traveling wave thermoacoustics in practice, The 19th International Conference on Sound and Vibration (ICSV19); July 8-12 2012. Vilnius, Lithuania.

[9] De Blok, K. Novel 4-stage traveling wave thermoacoustic power generator. In: Paper FEDSM2010-ICNMM2010-30527 in proc ASME 3rd joint US–European fluids

engineering summer meeting and 8th international conference on nanochannels, microchannels, and minichannels, Montreal, Canada 2010; August 2–4.

[10] Kongtragool B, Wongwises S. Thermodynamic analysis of a Stirling engine including dead volumes of hot space, cold space and regenerator. Renewable Energy 31, 2006; 345–359.

[11] Solanki R, Galindo A., Markides CN. Dynamic modelling of a two-phase thermofluidic oscillator for efficient low grade heat utilization: Effect of fluid inertia; Applied Energy 2012; 89 (1): 156-163.

[12] Piccolo A. Optimization of thermoacoustic refrigerators using second law analysis Applied Energy 2013; 103: 358–367.

[13] Yang, Z., Zhuo, Y., Luo, E.C. and Yuan, Z. Travelling-wave thermoacoustic high-temperature heat pump for industrial waste heat recovery. Energy, 2014, 77, 397-402.

[14] Xu, J., Hu, J., Zhang, L., Dai, W. & Luo, E. Effect of coupling position on a looped three-stage thermoacoustically-driven pulse tube cryocooler. Energy, 2015, 93, Part 1, 994-998.

[15] Xu, J., Zhang, L., Hu, J., Wu, Z., Bi, T., Dai, W. & Luo, E. An efficient looped multiple-stage thermoacoustically-driven cryocooler for liquefaction and recondensation of natural gas. Energy, 2016, 101, 427-433.

[16] Yu Z, Al-Kayiem A. Numerical analysis of a thermally driven thermoacoustic heat pump for low grade heat recovery. Computational Thermal Sciences 2014; 6(4): pp. 317-327.

[17] Yu, Z., and Jaworski, A.J. Optimization of thermoacoustic stacks for low onset temperature engines. Proceedings of the Institution of Mechanical Engineers Part A: Journal of Power and Energy, 2010, 224(3), pp. 329-337.

[18] Backhaus S, Tward E, Petach M. Traveling-wave thermoacoustic electric generator, Applied physics letters 2004; Volume 85: number 6.

[19] Petach M, Tward E, Backhaus S. Design and testing of a thermal to electric power converter based on thermoacoustic technology. In: 2nd International energy conversion engineering conference. The American Institute of Aeronautics and Astronautics, Providence, Rhode Island 2004; August 16–19.

[20] Oriti SM, Schifer NA. Recent Stirling conversion technology developments and operational measurements at NASA Glenn research centre. 7th International energy conversion and engineering conference (IECEC 2009); Denver, CO, August 2–5.

[21] Wu Z, Man M, Luo E, Dai W, Zhou Y. Experimental investigation of a 500 W traveling-wave thermoacoustic electricity generator. Chin Sci Bull 2011; 56:1975–7.

[22] Wu Z, Dai W, Man M, Luo E. A solar-powered traveling-wave thermoacoustic electricity generator. Sol Energy 2012; 86:2376–82.

[23] Sun D, Wang K, Zhang X, Guo Y, Xu Y, Qiu L. A traveling-wave thermoacoustic electric generator with a variable electric R-C load. Applied Energy 106, 2013; 377–382.

[24] Wu Z, Zhang L, Dai W, Luo E. Investigation on a 1 kW traveling-wave thermoacoustic electrical Generator. Applied Energy 2014; 124: 140–147.

[25] Wu Z, Yu G, Zhang L, Dai W, E. Development of a 3 kW double-acting thermoacoustic Stirling electric Generator Applied Energy 2014; 136: 866–872.

[26] Bi T., Wu Z., Zhang L., Yu G., Luo E., and Dai W. Development of a 5 kW traveling-wave thermoacoustic electric generator. Applied Energy. (in press)

[27] Wang K., Sun D., Zhang J., Xu Y., Zou J., Wu K., Qiu L., and Huang Z. Operating characteristics and performance improvements of a 500 W traveling-wave thermoacoustic electric generator. Applied Energy, 2015, 160, 853-862.

[28] Wang K., Sun D., Zhang J., Xu Y., Luo K., Zhang N., Zou J. and Qiu L. An acoustically matched traveling-wave thermoacoustic generator achieving 750 W electric power. Energy, 2016, 103, 313-321.

[29] Yu Z, Jaworski A, Backhaus S. A low-cost electricity generator for rural areas using a travelling-wave looped-tube thermoacoustic engine. Proceedings of the Institution of Mechanical Engineers, Part A: Journal of Power and Energy 2010; 224(6):787-795.

[30] Yu Z, Jaworski AJ, Backhaus S. Travelling-wave thermoacoustic electricity generator using an ultra-compliant alternator for utilization of low-grade thermal energy. Applied Energy 2012; 99:135-145.

[31] Kang H, Cheng P, Yu Z, Zheng H. A two-stage traveling-wave thermoacoustic electric generator with loudspeakers as alternators. Applied Energy 2015; 137: 9-17.

[32] Chen B.M., Riley P.H., Abakr Y.A., Pullen K., Hann D.B. and Johnson C.M.. Design and development of a low-cost, electricity-generating cooking Score-Stove™, Proceedings of the Institution of Mechanical Engineers, Part A: Journal of Power and Energy 2013; 227(7): 803-813.

[33] Chen B.M., Abakr Y.A., Riley P.H., Hann D.B., Development of thermoacoustic engine operating by waste heat from cooking stove, American.

[34] Chen B, Yousif A, Riley P, Hann D. Development and Assessment of Thermoacoustic Generators Operating by Waste Heat from Cooking Stove. Engineering 2012; 4: 894-902.

[35] Ward B, Clark J, Swift G. Design environment for low-amplitude thermoacoustic energy conversion, DELTAEC version 6.2: Users guide. Los Alamos national laboratory 2008.

[36] Swift G W. Thermoacoustics: A Unifying Perspective for Some Engines and Refrigerators. New York, Acoustical Society of America 2002.

[37] Hu J. Y., Ren J. , Luo E.C. and Dai W. Study on the inertance tube and double-inlet phase shifting modes in pulse tube refrigerators, Energy Conversion and Management, 52(2), 2011, 1077–1085

[38] Swift G. W. and Ward W. C. Simple Harmonic Analysis of regenerators, Journal of the thermophysics and heat transfer. 1996; 10 (4): 652-662

[39] Yu, Z, Jaworski A.J. Impact of acoustic impedance and flow resistance on the power output capacity of the regenerators in travelling-wave thermoacoustic engines. Energy Conversion and Management 2010; 51(2): 350-359.

[40] Kays W. M. and London A. L. Compact Heat Exchangers, Mcgraw-Hill, New York, (1964).

[41] Zhang X., Chang J., Cai S. and Hu J., A multi-stage travelling wave thermoacoustic engine driven refrigerator and operation features for utilizing low grade energy, Energy Conversion and Management, 2016, 114 , 224–233.

Table and Figure Captions

Table 1. The dimensions used in the present model of a bypass engine.

Table 2. The dimensions of the components of the thermally driven thermoacoustic cooler.

Table 3. Summary of the simulation results of the thermoacoustic engine driven cooler.

Figure 1. Schematic diagram of a travelling wave thermoacoustic engine with a bypass configuration [1]. The arrows indicate the direction of the acoustic power flow according to the simulations presented later in this paper. HHX: hot heat exchanger, REG: regenerator, AHX: ambient heat exchanger, TBT: thermal buffer tube.

Figure 2. Distribution of the amplitude of acoustic pressure along the engine. The solid square represents the measured data in the paper [1].

Figure 3. Distribution of the acoustic power along along the engine. The solid squares represent the measured data in the paper [1].

Figure 4. Distribution of the normalized specific acoustic impedance along the engine.

Figure 5. Phase angle θ between pressure and velocity oscillations along the engine.

Figure 6. Schematic diagram of the thermoacoustic engine driven cooler with a bypass configuration. HHX: hot heat exchanger, REG: regenerator, CHX: cold heat exchanger, AHX: ambient heat exchanger, TBT: thermal buffer tube.

Figure 7. Engine efficiency changes as the length of the regenerator varies.

Figure 8. Engine efficiency changes as the length of the bypass pipe varies.

Figure 9. Engine efficiency changes as the length of the phase shifting pipe varies.

Figure 10. Engine efficiency changes as the length of the compliance volume varies.

Figure 11. Engine efficiency changes as the length of the thermal buffer tube varies.

Figure 12. Distribution of the amplitude of acoustic pressure along the thermoacoustic engine driven cooler.

Figure 13. Distribution of the amplitude of volumetric velocity along the thermoacoustic engine driven cooler.

Figure 14. Distribution of the normalized specific acoustic impedance along the thermoacoustic engine driven cooler.

Figure 15. Phase angle θ between pressure and velocity oscillations along the thermoacoustic engine driven cooler.

Figure 16. Distribution of the acoustic power along the thermoacoustic engine driven cooler.

Table 1. The dimensions used in the present model of a bypass engine.

Part	Area (m^2)	Length(mm)	r_h (um)	Porosity
AHX1	0.012*	0.56†	40	0.8*
REG1	0.012*	1.58†	150	0.73*
HHX1	0.012*	0.56†	120	0.8*
AHX2	0.012*	0.56†	120	0.8*
REG2	0.012*	1.58†	130	0.73*
HHX2	0.012*	0.56†	120	0.8*
	Diameter (mm)		Length (cm)	
Bypass pipe	75*		100	
Feedback pipe	75*		175	
Phase shifting pipe	50*		120	
Compliance volume	110*		12.7	
Thermal buffer tube	100 mm× 120 mm*		3*	

*These dimensions were the same as those reported in the paper (*) and the associated conference presentation (†) [1].

Table 2. The dimensions of the components of the thermally driven thermoacoustic cooler.

Part	Diameter (cm)	Length (mm)	r_h (um)	Porosity
REG1	13.8	10	30	0.77
REG2	13.8	10	30	0.77
AHX1	13.8	21	700	0.5
AHX2	13.8	21	800	0.5
HHX1	13.8	20	800	0.51
CHX2	13.8	21	800	0.5

Part	Diameter (mm)	Length (cm)
Bypass pipe	55.2	120
Feedback pipe	71.3	308
Phase shifting pipe	42.2	120
Compliance volume	100.9	13.6
Thermal buffer tube	44.0	19

Table 3. Summary of the simulation results of the thermoacoustic engine driven cooler.

Symbol	Definition	Unit	Engine	Cooler
T_h	Solid Temperature of HHX	˚C	260	N/A
T_a	Solid Temperature of AHX	˚C	28	28
T_c	Solid Temperature of CHX	˚C	N/A	-19.1
$\dot{E}_{2,\,in}$	Acoustic power inlet	W	417.6	612.0
$\dot{E}_{2,\,out}$	Acoustic power outlet	W	613.0	452.5
$\dot{E}_{2,\,net}$	Net acoustic power production (engine) or consumption (cooler)	W	195.8	-159.5
$\dot{Q}_{in}$	Heat input to HHX (engine) or CHX (cooler)	W	1100.7	232.4
η_e	Engine Efficiency	%	14.5	
COP	Coefficient of performance (COP)		1.46	
η_{Carnot}	Carnot Efficiency: $(T_h\text{-}T_a)/T_h$	%	43.5	
COP_C	Carnot COP: $T_c/(T_a\text{-}T_c)$		5.4	
η_r	Percentage of Carnot Efficiency	%	33.4	
COP_R	Percentage of Carnot COP	%	27	

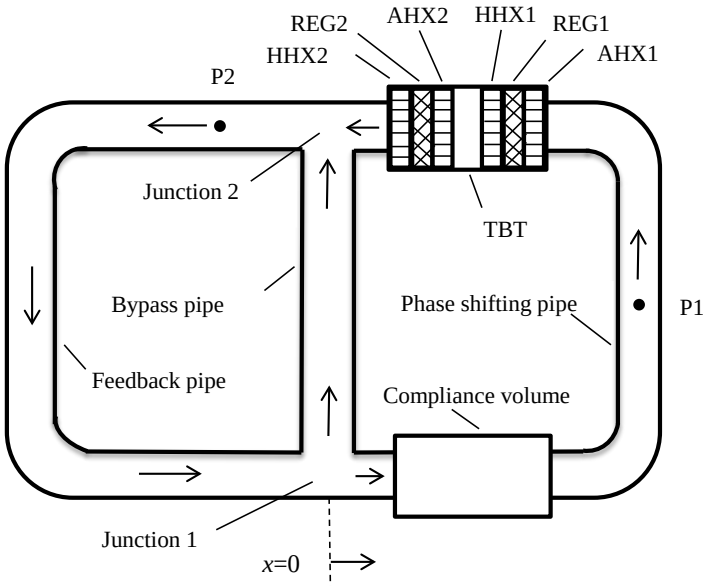

Figure 1. Schematic diagram of a travelling wave thermoacoustic engine with a bypass configuration [1]. The arrows indicate the direction of the acoustic power flow according to the simulations presented later in this paper. HHX: hot heat exchanger, REG: regenerator, AHX: ambient heat exchanger, TBT: thermal buffer tube.

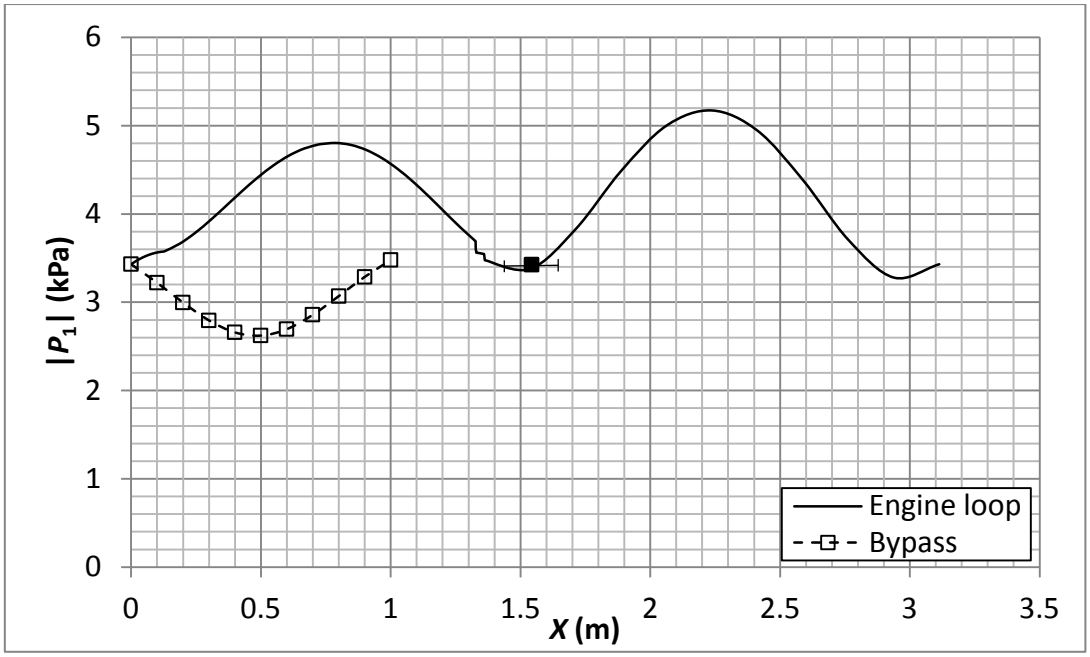

Figure 2. Distribution of the amplitude of acoustic pressure along the engine. The solid square represents the measured data in the paper [1].

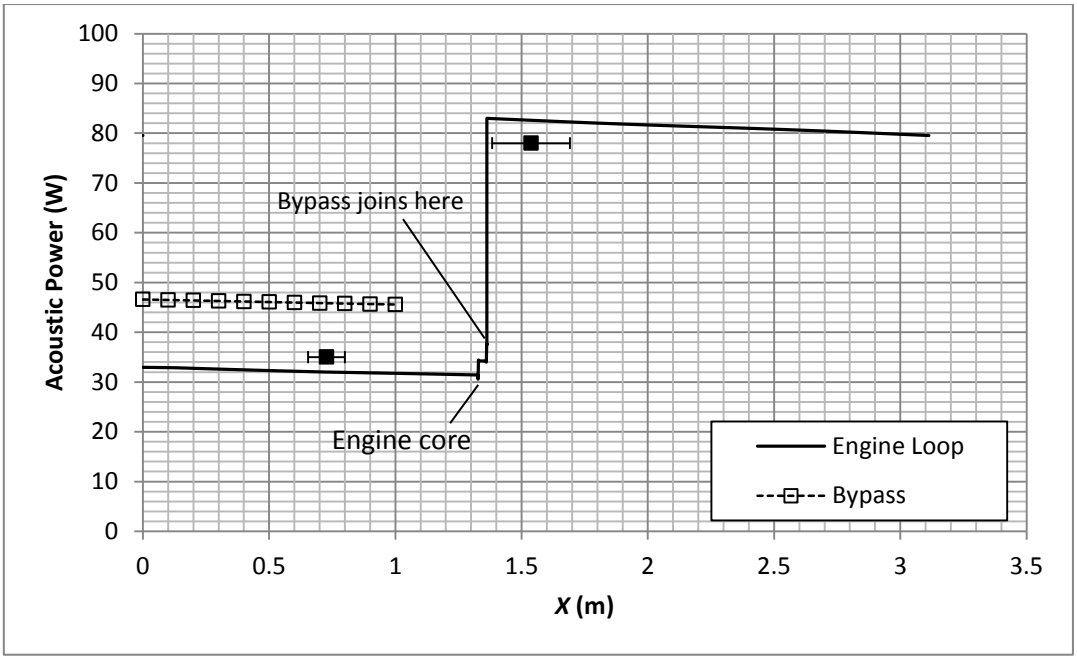

Figure 3. Distribution of the acoustic power along along the engine. The solid squares represent the measured data in the paper [1].

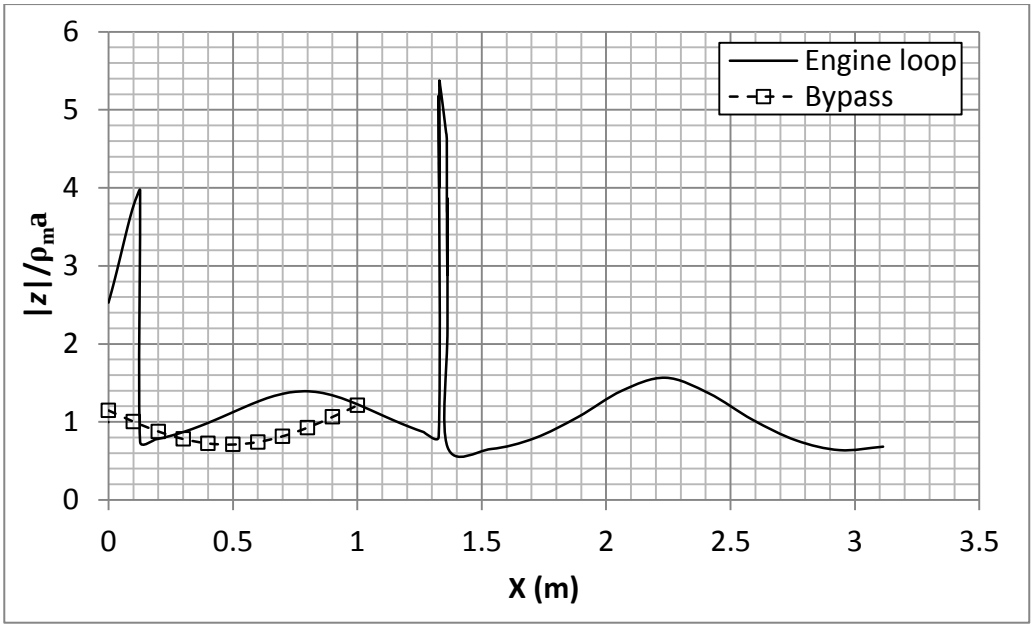

Figure 4. Distribution of the normalized specific acoustic impedance along the engine.

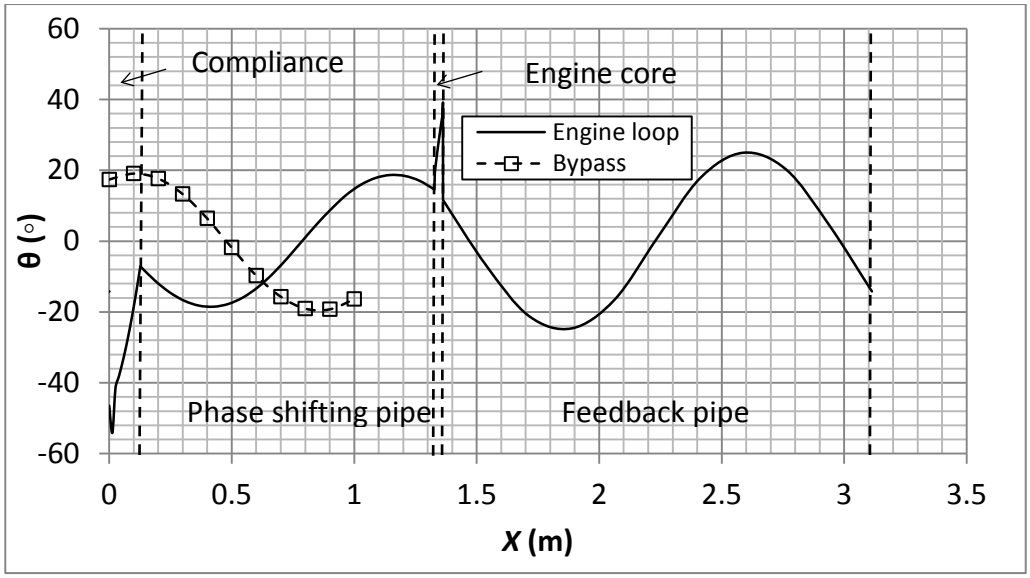

Figure 5. Phase angle θ between pressure and velocity oscillations along the engine.

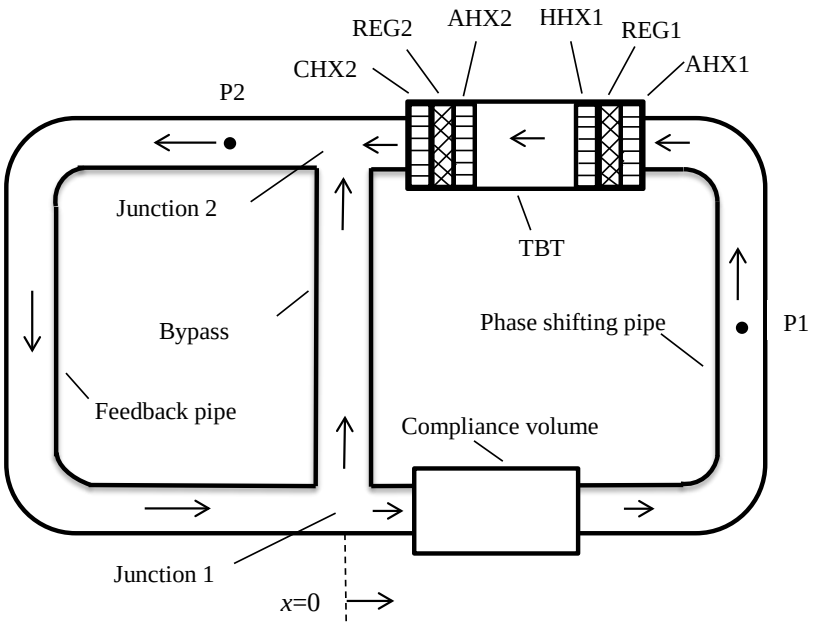

Figure 6. Schematic diagram of the thermoacoustic engine driven cooler with a bypass configuration. HHX: hot heat exchanger, REG: regenerator, CHX: cold heat exchanger, AHX: ambient heat exchanger, TBT: thermal buffer tube.

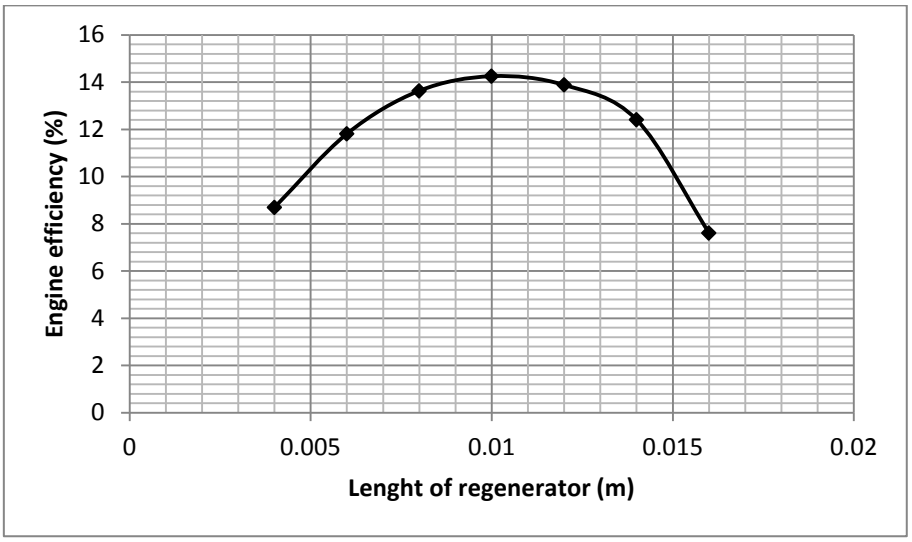

Figure 7. Engine efficiency changes as the length of the regenerator varies.

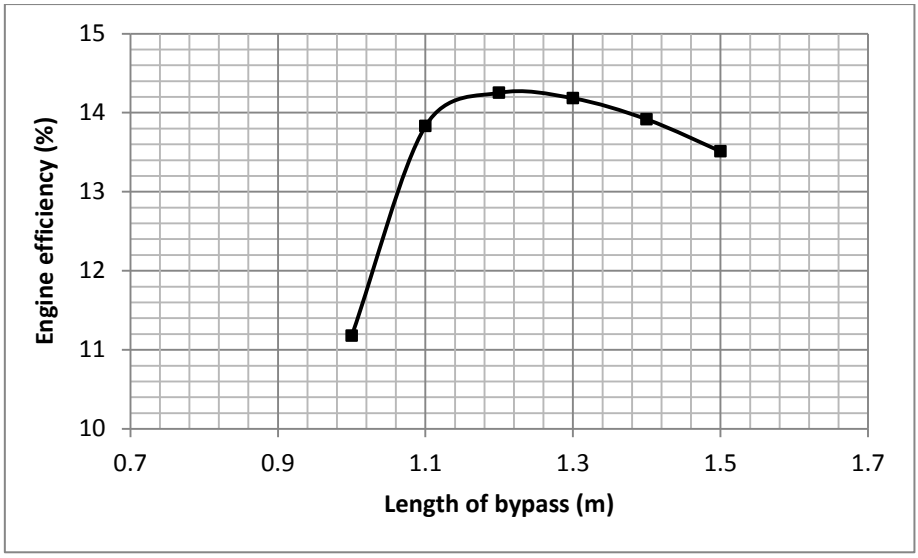

Figure 8. Engine efficiency changes as the length of the bypass pipe varies.

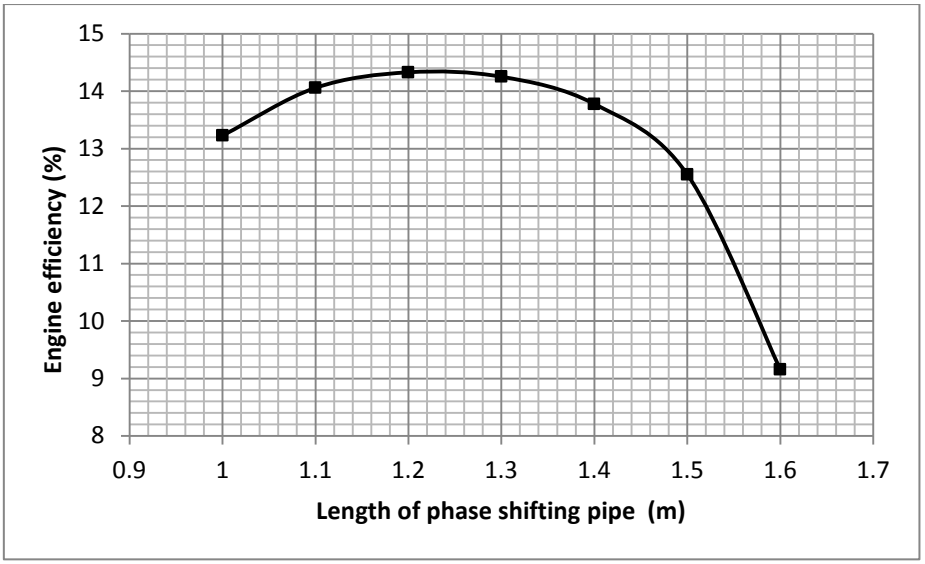

Figure 9. Engine efficiency changes as the length of the phase shifting pipe varies.

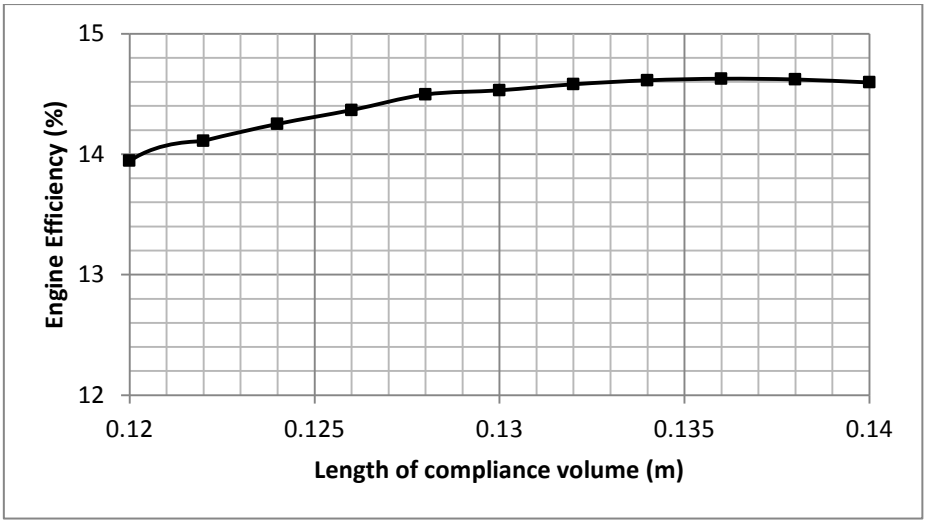

Figure 10. Engine efficiency changes as the length of the compliance volume varies.

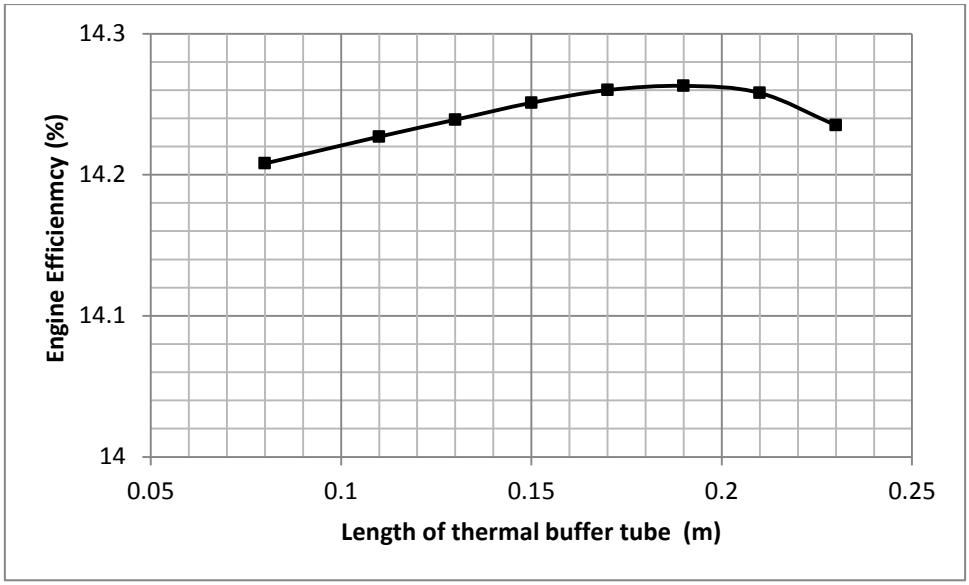

Figure 11. Engine efficiency changes as the length of the thermal buffer tube varies.

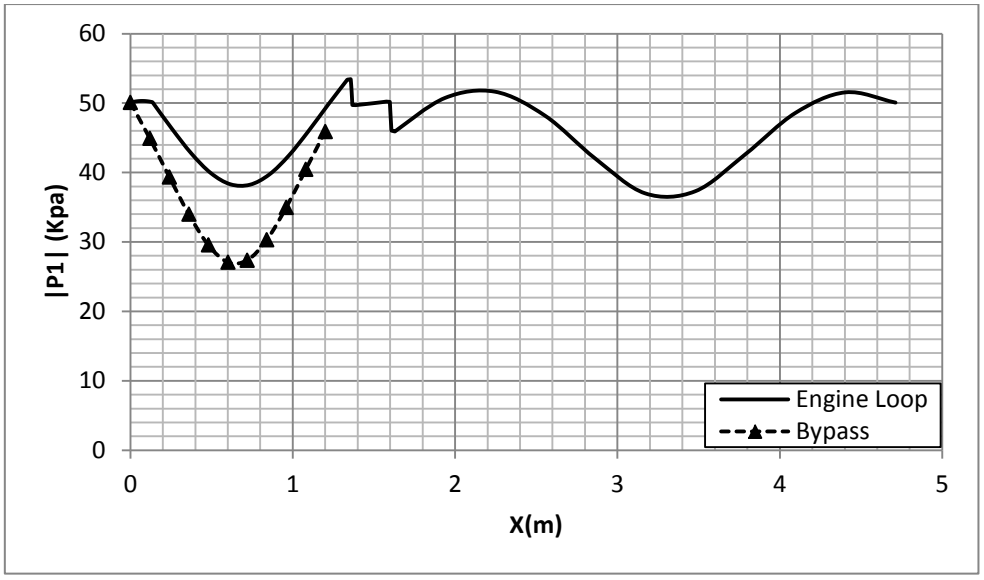

Figure 12. Distribution of the amplitude of acoustic pressure along the thermoacoustic engine driven cooler.

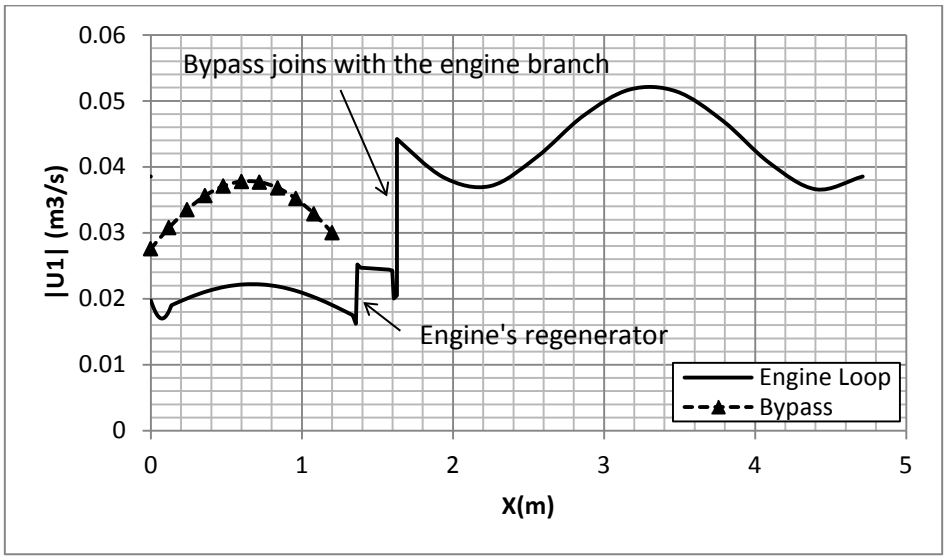

Figure 13. Distribution of the amplitude of volumetric velocity along the thermoacoustic engine driven cooler.

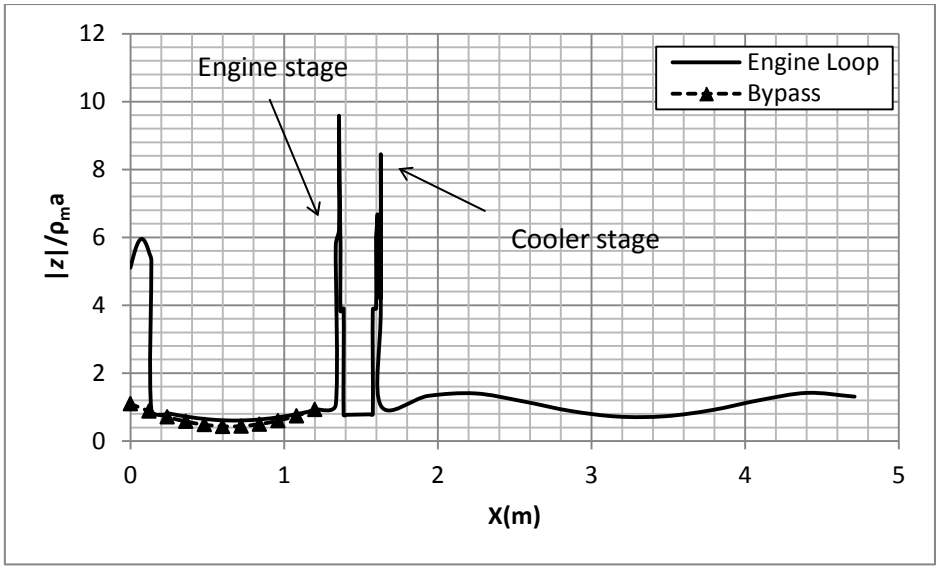

Figure 14. Distribution of the normalized specific acoustic impedance along the thermoacoustic engine driven cooler.

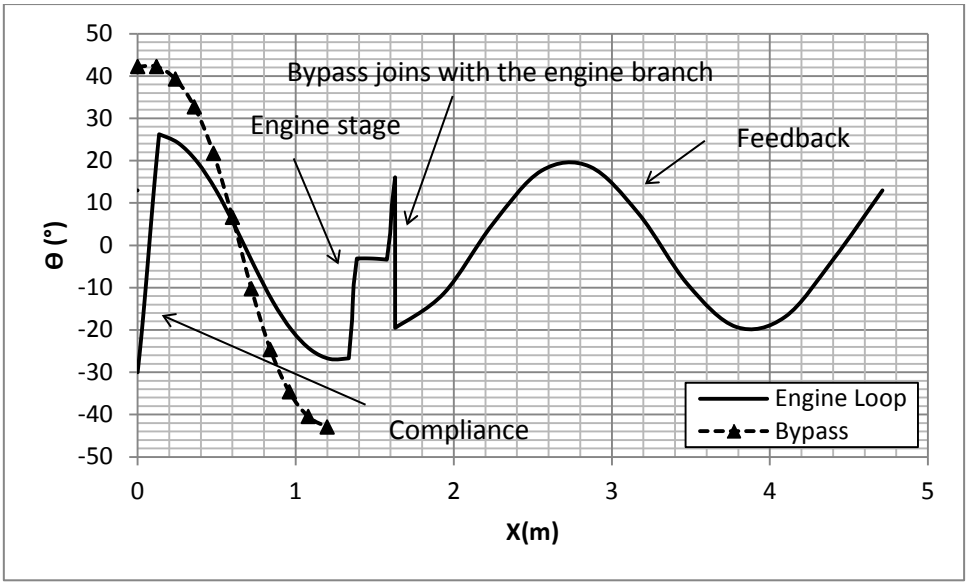

Figure 15. Phase angle θ between pressure and velocity oscillations along the thermoacoustic engine driven cooler.

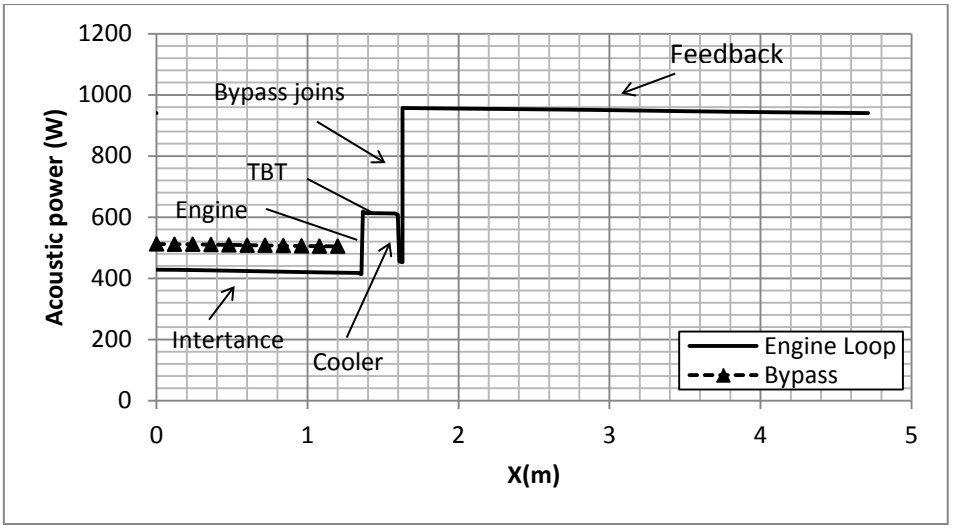

Figure 16. Distribution of the acoustic power along the thermoacoustic engine driven cooler.